Isolated attosecond pulses from Airy-beam-driven relativistic plasma mirrors

Peng Chen, Zeyue Pang, and Zi-Yu Chen ●*

Key Laboratory of High Energy Density Physics and Technology (MoE), College of Physics, Sichuan University, Chengdu 610064, China

Relativistically intense laser-driven plasma mirrors offer a promising route to produce attosecond pulses with high brightness. One major challenge is to generate an isolated attosecond pulse instead of a train of attosecond pulses when using multicycle driving lasers. Here we numerically demonstrate a scheme to achieve this goal by using Airy laser beams, whose main intensity self-bends transversely during propagation. The generated attosecond pulses are well separated in space and emitted in different directions. This scheme has the advantage of weak dependence on laser duration and thus is better suited for isolated attosecond pulse generation from a large class of conventional multicycle relativistic lasers worldwide.

I. INTRODUCTION

The development of intense attosecond light sources is a major goal in ultrafast science since it would allow real-time observation and even control of electronic dynamics in matter at the atomic scale [1–6]. High-order harmonic generation (HHG) from relativistically intense laser-irradiated solid-plasma surfaces has been suggested as a promising route to produce highly brilliant attosecond pulses [7], as plasma media have the advantage of overcoming the limitation of ionization in HHG from neutral gases [8] and damage in HHG from solid materials [9,10]. Experiments with HHG from laser plasmas at an intensity level of 10^{21} W/cm^2 have demonstrated impressive harmonic yields reaching $\sim$5 μJ and photon flux of $\sim 10^{12}$ photons/pulse at 3.1 keV (2600th order) in the spectral region of hard x rays [11].

The HHG mechanism in this regime is described as a relativistically oscillating mirror (ROM) model [11–15], which can be understood as a Doppler frequency upshift of laser light reflected off oscillating plasma surfaces. Such an oscillating mirror, driven under the combined action of laser ponderomotive force and charge-separation electrostatic force, can give rise to a burst of high-order harmonic pulses every laser optical cycle. Thus, a train of attosecond pulses is obtained when driven by multicycle lasers. Yet a single isolated attosecond pulse, rather than a train of pulses, is needed to perform attosecond time-resolved experiments.

Much effort has been devoted to generating an isolated attosecond pulse from relativistic plasma mirrors. A number of schemes have been investigated, such as shortening the laser temporal duration by developing relativistically intense few-cycle lasers [16–18], polarization gating methods that confine the HHG process within a time interval of about one optical cycle [19–22], noncollinear-gating [23] and attosecond-lighthouse [24,25] techniques that angularly streak the attosecond pulses in space, and some other

generation methods [26–29]. However, most schemes depend on laser pulse duration and become less effective for multicycle, long-duration ($\gtrsim$20 fs), high-intensity lasers, which form the majority of petawatt-class ($\gtrsim$200 TW) laser facilities worldwide. Hence, a method independent of, or weakly depending on, laser duration to generate an intense isolated attosecond pulse from many-cycle relativistic laser-driven plasma mirrors is highly desired.

In this work, we introduce Airy optical beams [30,31], instead of standard Gaussian beams, to deal with the problem. The Airy beam is a class of wave packets that have a transverse beam profile in the form of an Airy function. It was initially predicted by Berry and Balazs in 1979 as a solution to the potential-free Schrödinger equation describing a free particle [32]. Then it was exploited in the area of optics and experimentally realized by Siviloglou *et al.* in 2007 [33], as the paraxial equation describing optical waves,

$$i\frac{\partial \psi}{\partial \xi} + \frac{\partial^2 \psi}{2\partial s^2} = 0, \tag{1}$$

has some analogy with the Schrödinger equation mathematically, where ψ refers to the electric or magnetic field, $\xi = x/ky_0^2$ is a normalized propagation distance, $k = 2\pi/\lambda_L$ is the wave number of an optical wave with wavelength λ_L, y_0 is an arbitrary transverse scale, and $s = y/y_0$ is a dimensionless transverse coordinate.

Apart from the peculiar features of quasi-diffraction-free [30] and self-healing [34], a distinctive characteristic of Airy beams is self-acceleration [35]; i.e., the main intensity self-bends transversely with a curved trajectory as the beam propagates while maintaining its shape and intensity distribution. This unique property has been employed for diverse applications, such as on-chip synchrotron sources in the terahertz range [36], curved plasma channels and laser filamentation [37], three-dimensional superresolution fluorescence imaging [38], and optically mediated particle clearing [39].
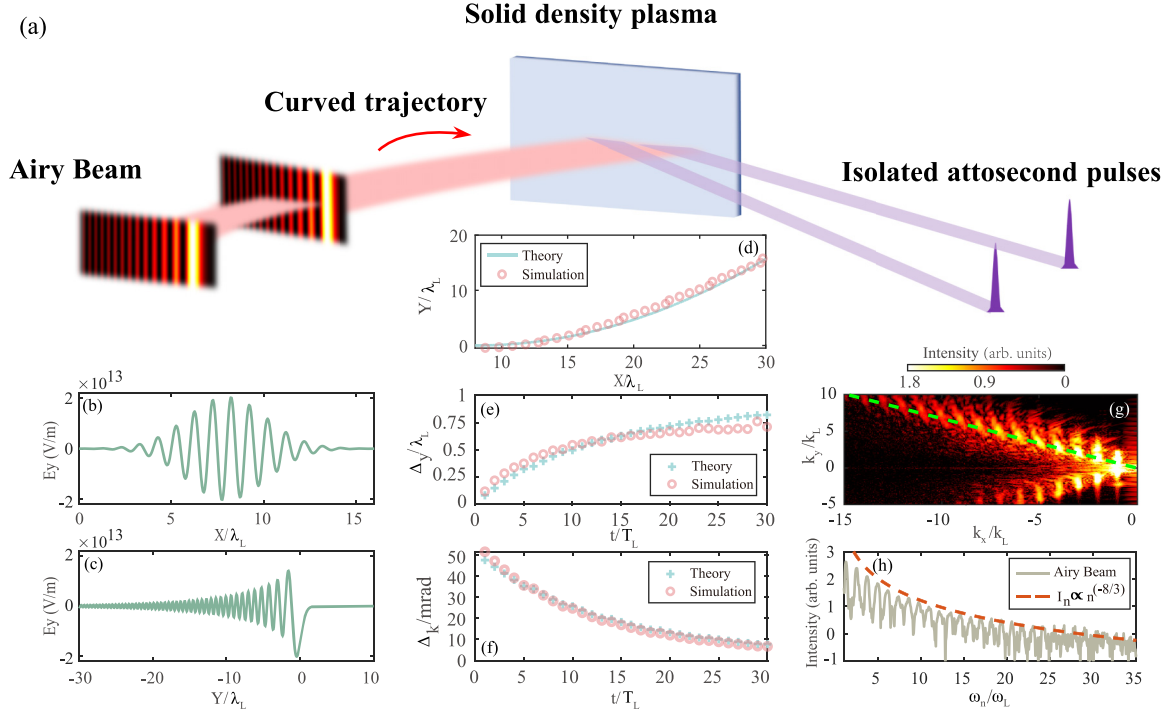
---

*ziyuch@scu.edu.cn

FIG. 1. (a) Scheme of spatially isolated attosecond pulse generation from Airy-beam-driven plasma surfaces. (b) Longitudinal electric-field wave form of the Airy beam, which has a Gaussian envelope. (c) Transverse electric-field wave form of the Airy beam, which can be described by an Airy function and an exponential decay profile. (d) Free-space propagation dynamics of the beam's main intensity in the XY plane, which exhibits a parabolic trajectory. The theoretical description is given by $y = x^2/(4k^2 y_0^3)$ [35]. (e) The lateral displacement of the main intensity in a time interval of one laser period as a function of propagation time. (f) The deflection angle of the laser wave vector in a time interval of one laser period for propagation. In (e) and (f), the theoretical results are calculated using the aforementioned equation of parabolic trajectory with simulated data as input. (g) Two-dimensional spatial Fourier transform of the high-order harmonic electric field. (h) High-order harmonic spectrum obtained with a 1D cut along the dashed line in (g). The normalized laser vector potential is $a_0 = 10$ (on-target peak field amplitude $E_L \approx 2.6$), and pulse duration is 14 fs ($\tau_L = 5T_L$). The plasma density is $n_e = 400n_c$, with density gradient $L_s = 0.08\lambda_L$. The target front surface is located at $x = 20\lambda_L$.

Here we exploit this self-bending property for isolated attosecond pulse generation from the plasma surface. The attosecond pulses can be emitted at different lateral locations on the plasma surface and propagate with different wave vectors during different laser optical cycles since the driving Airy beam undergoes transverse displacement during propagation. This should act like a streak camera to project the successively generated attosecond pulses along angularly separated paths and should lead to isolated attosecond pulses in the far field. A sketch of the scheme is shown in Fig. 1(a). We demonstrate this idea through two-dimensional (2D) particle-in-cell (PIC) simulations. We show that well spatially separated isolated attosecond pulses can be generated. The mechanism displays a robust performance for different laser durations.

II. SIMULATION SETUP

The 2D PIC simulations are performed using the code VLPL (Virtual Laser Plasma Lab) [40]. The initial electric field of the Airy laser beam, which propagates along the X axis, is given by

$$E = a_0 \text{Ai}\left(\frac{y}{y_0}\right) \exp\left(\frac{\beta y}{y_0}\right) \exp\left(\frac{-t^2}{2\tau_0^2}\right) \exp\left[-i(\mathbf{k} \cdot \mathbf{x} - \omega_L t)\right],$$

(2)

where $a_0 = eA_0/m_e c^2 = 10$ is the normalized laser vector potential, A_0 is the vector potential, ω_L is the laser angular frequency; e is the elementary charge; m_e is the electron mass; c is the speed of light in vacuum; $\text{Ai}(y/y_0)$ is the Airy function, with $y_0 = 0.5\lambda_L$ representing the transverse scale; $\beta = 0.05$ is a small positive decay parameter to ensure the Airy wave packet has finite energy; and τ_0 is related to the full width at half maximum (FWHM) pulse duration as $\tau_L = 2\sqrt{2\ln 2}\,\tau_0$. Because the peak value of the Airy function is less than 1 and the diffraction effect occurs during propagation, the peak laser electric-field amplitude E_L (normalized by $m_e c \omega_L/e$) drops to about 2.6 at the target surface. The laser pulse has a sinusoidal field and Gaussian envelope for the temporal profile, as shown in Fig. 1(b) for the initial longitudinal electric field. In the transverse direction, the laser field has a wave form of an Airy function and an exponential decay profile, as depicted in Fig. 1(c). The transverse intensity profile thus has an extended main lobe and a series of smaller lobes trailing behind it. The curved propagation is associated with this parity-asymmetric field pattern [41].

In experiments, 1D (2D) Airy beams can be generated by first imposing a cubic spatial phase on Gaussian beams in one (two) transverse dimension(s) by using a spatial light modulator [33] since the Airy function forms a Fourier transform pair with the Gaussian function modulated by a cubic spatial

phase. Other ways to impose phase modulation, such as using metamaterials [42] or photon crystals [43], have also been demonstrated. Then the 1D (2D) phase-modulated Gaussian beam can be subsequently focused in that (those) dimension(s) to obtain 1D (2D) Airy beams reaching relativistic intensity. A similar approach was employed to successfully generate relativistically intense vector beams in experiments [44]. In practice, in order to reach high intensity, 2D rather than 1D Airy beams that are focused in both transverse dimensions are required. Here we only simulate 1D Airy beams since they can capture the relevant aspects of 2D beams because the Airy function, as the only dispersion-free solution in one dimension [32], allows space and time decoupling of the wave packets [45]. Thus, each transverse component of 2D Airy beams behaves independently and equivalently upon propagation.

The fully ionized plasma consists of a preplasma region and a plasma slab. The preplasma has a thickness of $1.5\lambda_L$ and an exponential density distribution $n_e = n_0 \exp\left[-(x_0 - x)/L_s\right]$, where $n_c = m_e\omega_L/(4\pi e^2)$ is the plasma critical density, $L_s = 0.08\lambda_L$ is the preplasma scale length, and x_0 denotes the end (start) position of the preplasma (plasma slab). The plasma slab has a thickness of $0.5\lambda_L$ and homogeneous density of $n_0 = 400n_c$. The ions are considered immobile in the simulations.

The size of the simulation box is $X \times Y = 24.6\lambda_L \times 60\lambda_L$, where $\lambda_L = 800$ nm is the laser wavelength. The grid step size in both directions is $\lambda_L/200$, and the time step is $0.0035T_L$, with T_L being the laser period. Each cell is filled with 16 macroparticles. Absorption boundary condition is applied to both fields and particles.

III. RESULTS AND DISCUSSION

Figures 1(d)–1(f) show the propagation dynamics of the Airy beam in free space. The motion of the beam's main intensity (the first lobe) follows a characteristic curved trajectory [see Fig. 1(d)], in good agreement with the theoretical description of parabolic deflection given by [35]

$$y = \frac{1}{2}gx^2, \quad g = \frac{1}{2k^2y_0^3}, \tag{3}$$

where g plays the role of "gravity." This self-acceleration behavior implies that (1) the beam's main intensity center undergoes a lateral displacement and (2) the direction of the laser wave vector continuously changes during propagation. As can be seen from Fig. 1(e), the lateral position of the beam's main intensity shifts more than half a laser wavelength in a time interval of one laser optical period T_L after a propagation time of $10T_L$. At the same time, the deflection angle Δ_k of the wave-vector direction during every laser period can reach about a few tens of milliradians, as depicted in Fig. 1(f). The simulated results for lateral displacement and wave-vector deflection agree well with those calculated using Eq. (3). Both aspects are helpful for spatial separation of the attosecond pulses in the far field.

To enable spatial separation, the angular offset between two successive attosecond pulses $\Delta\theta$ should be larger than the divergence angle θ_n of the nth harmonic beam: $\Delta\theta > \theta_n$. For diffraction-limited high-order harmonics with the same source

size as the laser's, the divergence for an individual harmonic can be estimated with the laser divergence θ_L as $\theta_n \sim \theta_L/n$. As a rough estimation, if the laser divergence is $\theta_L \sim 20°$ [46], then for high-order harmonics with order $n > 20$, we obtain $\theta_n \sim 1°$, corresponding to $\theta_n \sim 17$ mrad. From Fig. 1(f), we see the laser deflection angle $\Delta_k < 20$ mrad after a propagation time of $\sim 13T_L$. However, as we will show later, the resultant angular offset of attosecond pulses $\Delta\theta$ can be larger than the theoretical laser wave-vector deflection angle Δ_k, allowing the spatial separation condition to be fulfilled.

Figure 1(g) shows the 2D spatial Fourier transform of the reflected electric field in the vacuum region after the interaction, where the incident laser FWHM duration τ_L is five optical cycles, corresponding to ~ 14 fs. The harmonic components with $k_y > 0$ are generated by the main lobe of the Airy beam containing most of the energy of the pulse, while the other harmonic components with $k_y < 0$ result from the less intense sidelobes of the driving pulse.

Figure 1(h) illustrates the harmonic spectrum obtained with a 1D cut along the dashed line in Fig. 1(g). A well-defined harmonic structure extending to about 30th order is generated. The spectral intensity as a function of harmonic order agrees well with the theoretically predicted scaling law $I(n) \propto n^{-8/3}$ from the γ-spike model [14], suggesting the HHG mechanism here is in the ROM regime. Harmonics with both odd and even orders can be observed, although the Airy beam is at normal incidence initially. This indicates that the laser wave vector changes direction as it self-bends during propagation. Hence, the actual interaction is under the geometry of oblique incidence, which allows HHG once per laser period with a higher efficiency [13]. The normal-incidence setup is chosen for the sake of simplicity and thus is not optimized.

Figures 2(a)–2(c) show the spatial distribution of the attosecond pulse intensity and plasma density around the emission time for three successive attosecond pulses. The laser duration is $\tau_L = 5T_L$. The attosecond pulses are obtained after spectral filtering by selecting harmonic orders $n \geqslant 20$. The attosecond pulses originate from the dense electron bunches forming at the plasma front surface moving towards the field reflection direction. The attosecond pulses are spatially separated by $\sim 1\lambda_L$ in the transverse direction, consistent with the lateral displacement of the Airy beam. Figures 2(d)–2(f) show the spatial distribution of plasma density and intensity for one of the attosecond pulses at three different times during emission. It is clear that the plasma-denting effect is small, and the attosecond pulse emission is not evidently focused by the plasma mirror within our parameter regime.

To investigate the propagation properties of the attosecond pulses, we trace the center of energy of representative attosecond pulses for a series of propagation times. Figures 3(a)–3(d) show the results for driving-laser duration τ_L from five optical cycles (~ 14 fs) to eight cycles (~ 22 fs). One notable feature is that the motion trajectory of each isolated attosecond pulse follows a straight line, in contrast to the parabolic deflection of the driving Airy beam. This is because the target is placed some distance away from the initial Airy-beam positions. This allows the Airy beams to diffract for some time, so that the isolated attosecond pulses are generated only by the main intensity lobe of the Airy beam, while the harmonics generated
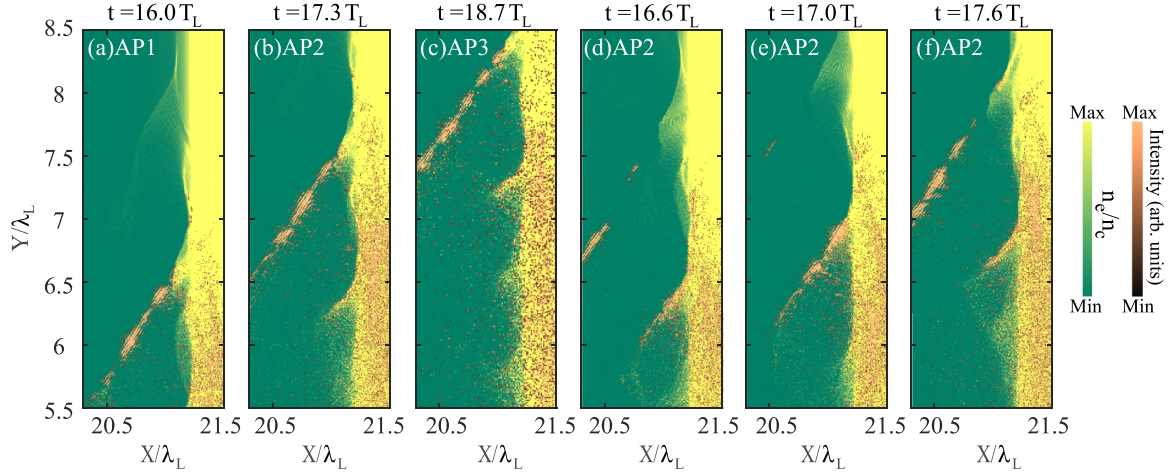
FIG. 2. Spatial distribution of attosecond pulse intensity (black-orange scale) and plasma density (green-yellow scale) around the emission time instant for [(a)–(c)] three successive attosecond pulses and [(d)–(f)] one of the attosecond pulses (AP2) at three different times during emission. The attosecond pulses are obtained after spectral filtering by selecting harmonics with order $n \geqslant 20$. The other parameters are the same as those in Fig. 1.

by the more diffracted and less intense sidelobes diverge rapidly with further propagation. Consequently, the isolated attosecond pulse no longer exhibits an Airy-beam profile. Through linear fitting, we obtain the angle θ between the line along the propagation path and the X axis for each isolated attosecond pulse. We find that each isolated attosecond pulse propagates along a different direction as a result of the varying wave vector of the Airy beam during the interaction. The

maximum angular offset $\Delta\theta$ between two successive attosecond pulses can reach about 50, 60, 60, and 40 mrad for laser durations of five, six, seven, and eight cycles, respectively, larger than the laser wave-vector variation in Fig. 1(f), which may be caused by the attosecond pulse emission process accompanied by the simultaneous dynamical effects of laser lateral shifting and electron bunch oscillating, as shown in Fig. 2.
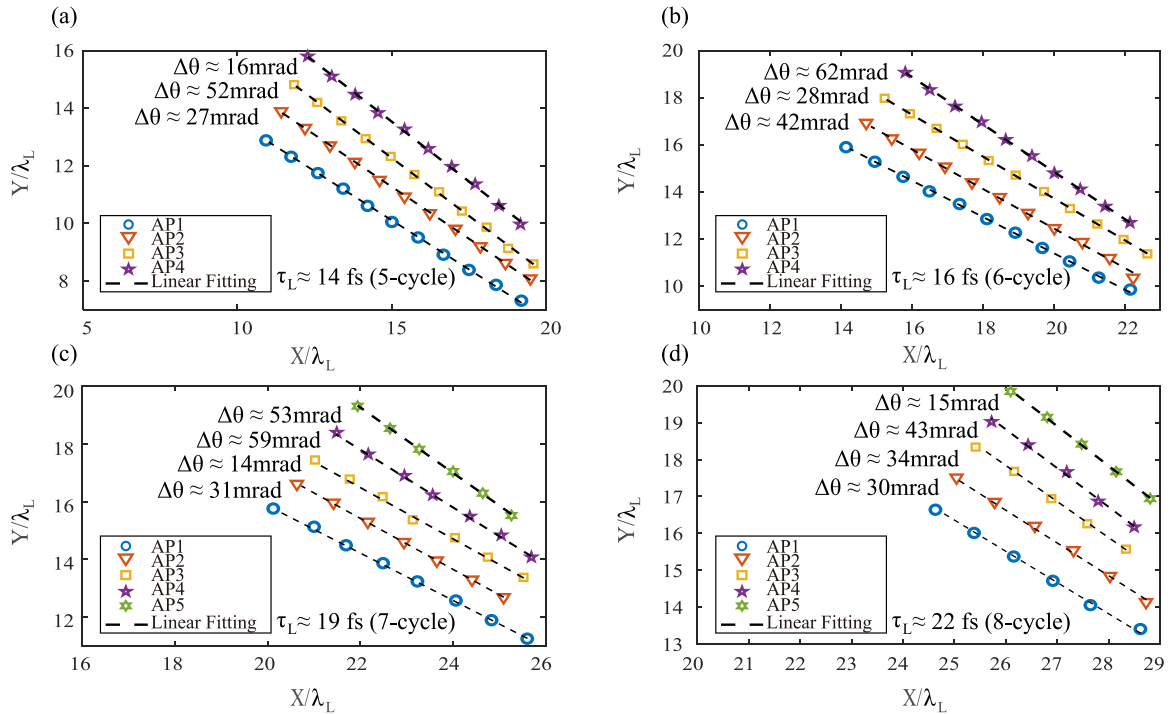

FIG. 3. Propagation dynamics of the center of energy of each attosecond pulse (AP) for a series of propagation times. The driving-laser FWHM duration τ_L is (a) $5T_L$ ($\sim$14 fs), (b) $6T_L$ ($\sim$16 fs), (c) $7T_L$ ($\sim$19 fs), and (d) $8T_L$ ($\sim$22 fs). The dashed lines describe linear fitting. $\Delta\theta$ is obtained by calculating the difference in the angle between the propagation direction of the AP and the X axis. The AP is obtained with harmonic order $n \geqslant 20$. The target front surface is at $x = 23\lambda_L$, $26\lambda_L$, $29\lambda_L$ for [(b)–(d)], respectively, to ensure the same laser intensity reaches the target surface. The other parameters are the same as those in Fig. 1.

TABLE I. Harmonic ($n \geqslant 20$) source size w_n in the plasma mirror plane obtained from PIC simulations and the calculated harmonic divergence θ_n for each attosecond pulse (AP) driven by lasers with different durations τ_L. The laser beam size in the plasma mirror plane is $w_L = 1.4\lambda_L$.

τ_L (in units of T_L)																	
5	5	5	5	6	6	6	6	7	7	7	7	7	8	8	8	8	8
AP No. 1	2	3	4	1	2	3	4	1	2	3	4	5	1	2	3	4	5
w_n (λ_L) 1.2	1.2	1.0	0.9	0.9	1.1	1.1	0.8	1.0	1.0	1.0	0.9	0.8	1.2	1.2	1.2	1.2	0.8
θ_n (mrad) 15	15	22	28	28	18	18	35	22	22	22	28	35	15	15	15	15	35

To enable an angularly separated isolated attosecond pulse in the far field, the condition $\Delta\theta > \theta_n$ should be fulfilled. Since with our parameters the plasma denting is negligible, considering the effect of harmonic-source-size shrinkage due to nonlinearity, the harmonic divergence can be calculated as [47]

$$\theta_n = \frac{w_L}{w_n} \frac{\lambda_n}{\pi w_n}, \qquad (4)$$

where λ_n is the nth harmonic wavelength and w_L and w_n are the laser and harmonic beam sizes in the plasma mirror plane, respectively. In our simulations, we find $w_L = 1.4\lambda_L$ and $w_n = 0.8 - 1.2\lambda_L$, and thus, the calculated harmonic divergence θ_n ranges from 15 to 35 mrad for different attosecond pulses driven by lasers with duration $\tau_L = 5T_L–8T_L$, as shown in Table I. Most harmonics have a divergence of around 20 mrad, in agreement with the experimental results of ∼19 mrad by Dromey *et al.* using a similar laser amplitude [46]. As a result, multiple attosecond pulses satisfying $\Delta\theta > \theta_n$ exist for each case of laser duration from five to eight cycles. This demonstrates angularly well separated isolated attosecond pulses in the far field can be obtained with a driving-laser duration above the level of 20 fs, within the range of realistic multicycle high-power lasers.

A snapshot of the 2D spatial intensity profile of the attosecond pulses after they propagate away from the target area at $t = 46T_L$ for $\tau_L = 8T_L$ is shown in Fig. 4(a). The harmonic orders are $n \geqslant 20$. A group of spatially separated isolated attosecond pulses can be obtained by applying slit filters in the far field since $\Delta\theta > \theta_n$. Figures 4(b) and 4(c) show, respectively, the 1D temporal (longitudinal) and spatial (transverse) intensity profiles of one attosecond pulse [AP3 in Fig. 4(a)]. A Gaussian fitting gives a duration (FWHM) of the attosecond pulse of ∼190 as and beam size ($1/e^2$) of ∼$1\lambda_L$.

The dependence of the driving-laser duration and spatial isolation patterns of the attosecond pulses in Fig. 3 is weak since the key elements of the scheme, i.e., lateral displacement and wave-vector deflection, are due to the inherent properties of Airy beams. This suggests working with even longer laser duration may be possible. The mechanism here is different from that of the attosecond-lighthouse technique, which is based on using spatiotemporally coupled light fields exhibiting wave-front rotation. As the wave-vector rotation speed is limited by the pulse duration, the lighthouse technique usually needs few-cycle pulses to achieve sufficient angular separation between attosecond pulses. In addition, the attosecond pulses generated by the lighthouse scheme may also inherit the spatiotemporal coupling feature of the driving laser. In comparison, the attosecond pulses in the present scheme are decoupled in space and time.

The scheme was tested and found to work well for higher laser strength (e.g., with $a_0 = 20$ initially and $E_L \approx 5.2$ on the target surface). However, it will eventually fail at sufficiently high laser intensity because severe plasma denting induced by laser radiation pressure inevitably occurs. The high-order harmonic divergence is enhanced so greatly that the spatial separation condition $\Delta\theta > \theta_n$ is no longer satisfied. This is the common difficulty other spatial separation schemes also encounter [23,48]. In this case, other recently proposed methods, such as further increasing plasma density [23], placing the target off the best focus, [48] and optical plasma-surface shaping [49], can be employed jointly with the Airy beam to
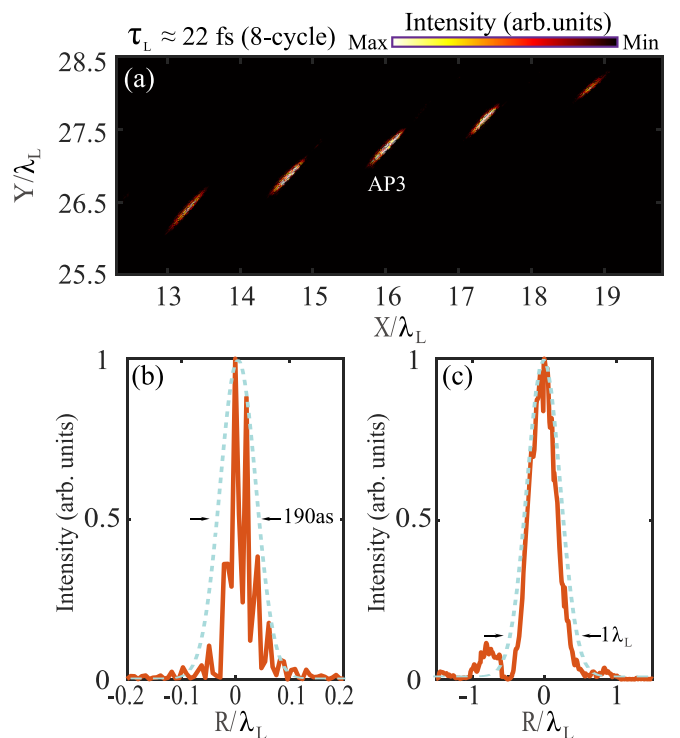

FIG. 4. (a) A snapshot of the spatial intensity profile of the attosecond pulses with harmonic order $n \geqslant 20$ at $t = 46T_L$. The driving-laser duration is $\tau_L = 8T_L$ (∼22 fs). The target surface is at $x = 29\lambda_L$. One-dimensional profile of the (b) temporal and (c) spatial intensity distributions of one isolated attosecond pulse [AP3 in (a)]. R denotes the coordinate along the 1D cut line. The other parameters are the same as those in Fig. 1.

suppress the plasma denting and subsequent harmonic divergence effects.

IV. CONCLUSIONS

In conclusion, an alternative scheme to obtain isolated attosecond pulses from relativistic plasma mirrors based on using an Airy beam was proposed and demonstrated through 2D PIC simulations. The nonlinear propagation effects and curved trajectories of the Airy beam lead to transverse displacement and wave-vector deflection of the main intensity, which result in spatially separated attosecond pulses. This mechanism releases constraints on laser pulse duration and

works for relativistically intense lasers with realistic FWHM durations $\gtrsim 20$ fs, paving the way towards the generation of a bright isolated attosecond pulse for ultrafast science from a large class of multicycle high-power laser facilities worldwide.

[1] M. Drescher, M. Hentschel, R. Kienberger, M. Uiberacker, V. Yakovlev, A. Scrinzi, Th. Westerwalbesloh, U. Kleineberg, U. Heinzmann, and F. Krausz, Time-resolved atomic inner-shell spectroscopy, Nature (London) **419**, 803 (2002).

[2] F. Calegari, D. Ayuso, A. Trabattoni, L. Belshaw, S. De Camillis, S. Anumula, F. Frassetto, L. Poletto, A. Palacios, P. Decleva, J. B. Greenwood, F. Martín, and M. Nisoli, Ultrafast electron dynamics in phenylalanine initiated by attosecond pulses, Science **346**, 336 (2014).

[3] F. Krausz and M. Ivanov, Attosecond physics, Rev. Mod. Phys. **81**, 163 (2009).

[4] A. L. Cavalieri, N. Müller, Th. Uphues, V. S. Yakovlev, A. Baltuška, B. Horvath, B. Schmidt, L. Blümel, R. Holzwarth, S. Hendel, M. Drescher, U. Kleineberg, P. M. Echenique, R. Kienberger, F. Krausz, and U. Heinzmann, Attosecond spectroscopy in condensed matter, Nature (London) **449**, 1029 (2007).

[5] G. Sansone, F. Kelkensberg, J. F. Pérez-Torres, F. Morales, M. F. Kling, W. Siu, O. Ghafur, P. Johnsson, M. Swoboda, E. Benedetti, F. Ferrari, F. Lépine, J. L. Sanz-Vicario, S. Zherebtsov, I. Znakovskaya, A. L'Huillier, M. Yu. Ivanov, M. Nisoli, F. Martín, and M. J. J. Vrakking, Electron localization following attosecond molecular photoionization, Nature (London) **465**, 763 (2010).

[6] M. Schultze, M. Fies, N. Karpowicz, J. Gagnon, M. Korbman, M. Hofstetter, S. Neppl, A. L. Cavalieri, Y. Komninos, Th. Mercouris *et al.*, Delay in photoemission, Science **328**, 1658 (2010).

[7] U. Teubner and P. Gibbon, High-order harmonics from laser-irradiated plasma surfaces, Rev. Mod. Phys. **81**, 445 (2009).

[8] C. Winterfeldt, C. Spielmann, and G. Gerber, *Colloquium*: Optimal control of high-harmonic generation, Rev. Mod. Phys. **80**, 117 (2008).

[9] S. Ghimire, A. D. DiChiara, E. Sistrunk, P. Agostini, L. F. DiMauro, and D. A. Reis, Observation of high-order harmonic generation in a bulk crystal, Nat. Phys. **7**, 138 (2011).

[10] S. Ghimire and D. A. Reis, High-harmonic generation from solids, Nat. Phys. **15**, 10 (2019).

[11] B. Dromey, S. Kar, C. Bellei, D. C. Carroll, R. J. Clarke, J. S. Green, S. Kneip, K. Markey, S. R. Nagel, P. T. Simpson, L. Willingale, P. McKenna, D. Neely, Z. Najmudin, K. Krushelnick, P. A. Norreys, and M. Zepf, Bright multi-keV

harmonic generation from relativistically oscillating plasma surfaces, Phys. Rev. Lett. **99**, 085001 (2007).

[12] S. V. Bulanov, N. M. Naumova, and F. Pegoraro, Interaction of an ultrashort, relativistically strong laser pulse with an overdense plasma, Phys. Plasmas **1**, 745 (1994).

[13] R. Lichters, J. Meyer-ter-Vehn, and A. Pukhov, Short-pulse laser harmonics from oscillating plasma surfaces driven at relativistic intensity, Phys. Plasmas **3**, 3425 (1996).

[14] T. Baeva, S. Gordienko, and A. Pukhov, Theory of high-order harmonic generation in relativistic laser interaction with overdense plasma, Phys. Rev. E **74**, 046404 (2006).

[15] B. Dromey, M. Zepf, A. Gopal, K. Lancaster, M. S. Wei, K. Krushelnick, M. Tatarakis, N. Vakakis, S. Moustaizis, R. Kodama, M. Tampo, C. Stoeckl, R. Clarke, H. Habara, D. Neely, S. Karsch, and P. Norreys, High harmonic generation in the relativistic limit, Nat. Phys. **2**, 456 (2006).

[16] D. Kormin, A. Borot, G.-J. Ma, W. Dallari, B. Bergues, M. Aladi, I. B. Földes, and L. Veisz, Spectral interferometry with waveform-dependent relativistic high-order harmonics from plasma surfaces, Nat. Commun. **9**, 4992 (2018).

[17] O. Jahn, V. E. Leshchenko, P. Tzallas, A. Kessel, M. Krüger, A. Münzer, S. A. Trushin, G. D. Tsakiris, D. Kahaly, S. Kormin, L. Veisz, V. Pervak, F. Krausz, Z. Major, and S. Karsch, Towards intense isolated attosecond pulses from relativistic surface high harmonics, Optica **6**, 280 (2019).

[18] F. Böhle, M. Thévenet, M. Bocoum, A. Vernier, S. Haessler, and R. Lopez-Martens, Generation of XUV spectral continua from relativistic plasma mirrors driven in the near-single-cycle limit, J. Phys. Photon. **2**, 034010 (2020).

[19] S. G. Rykovanov, M. Geissler, J. Meyer-ter Vehn, and G. D. Tsakiris, Intense single attosecond pulses from surface harmonics using the polarization gating technique, New J. Phys. **10**, 025025 (2008).

[20] M. Yeung, B. Dromey, S. Cousens, T. Dzelzainis, D. Kiefer, J. Schreiber, J. H. Bin, W. Ma, C. Kreuzer, J. Meyer-ter-Vehn, M. J. V. Streeter, P. S. Foster, S. Rykovanov, and M. Zepf, Dependence of laser-driven coherent synchrotron emission efficiency on pulse ellipticity and implications for polarization gating, Phys. Rev. Lett. **112**, 123902 (2014).

[21] M. Yeung, J. Bierbach, E. Eckner, S. Rykovanov, S. Kuschel, A. Sävert, M. Förster, C. Rödel, G. G. Paulus, S. Cousens, M. Coughlan, B. Dromey, and M. Zepf, Noncollinear polarization

gating of attosecond pulse trains in the relativistic regime, Phys. Rev. Lett. **115**, 193903 (2015).

[22] Z.-Y. Chen, X.-Y. Li, B.-Y. Li, M. Chen, and F. Liu, Isolated elliptically polarized attosecond soft x-ray with high-brilliance using polarization gating of harmonics from relativistic plasmas at oblique incidence, Opt. Express **26**, 4572 (2018).

[23] J. P. Kennedy, B. Dromey, and M. Yeung, Isolated ultra-bright attosecond pulses via non-collinear gating, New J. Phys. **24**, 113004 (2022).

[24] H. Vincenti and F. Quéré, Attosecond lighthouses: How to use spatiotemporally coupled light fields to generate isolated attosecond pulses, Phys. Rev. Lett. **108**, 113904 (2012).

[25] J. A. Wheeler, A. Borot, S. Monchocé, H. Vincenti, A. Ricci, A. Malvache, R. Lopez-Martens, and F. Quéré, Attosecond lighthouses from plasma mirrors, Nat. Photon. **6**, 829 (2012).

[26] N. M. Naumova, J. A. Nees, I. V. Sokolov, B. Hou, and G. A. Mourou, Publisher's note: Relativistic generation of isolated attosecond pulses in a λ^3 focal volume [Phys. Rev. Lett. **92**, 063902 (2004)], Phys. Rev. Lett. **92**, 089901(E) (2004).

[27] Z.-Y. Chen, Isolated attosecond pulse in the water window from many-cycle laser-driven plasma mirrors without pulse engineering, Opt. Lett. **43**, 2114 (2018).

[28] M. Blanco and M. T. Flores-Arias, Frequency gating to isolate single attosecond pulses with overdense plasmas using particle-in-cell simulations, Opt. Express **25**, 13372 (2017).

[29] Q.-N. Li, X.-R. Xu, Y.-B. Wu, D.-B. Zhou, Y. Yin, and T.-P. Yu, Generation of single circularly polarized attosecond pulses from near-critical density plasma irradiated by a two-color co-rotating circularly polarized laser, Opt. Express **30**, 40063 (2022).

[30] G. A. Siviloglou and D. N. Christodoulides, Accelerating finite energy Airy beams, Opt. Lett. **32**, 979 (2007).

[31] N. K. Efremidis, Z.-G. Chen, M. Segev, and D. N. Christodoulides, Airy beams and accelerating waves: An overview of recent advances, Optica **6**, 686 (2019).

[32] M. V. Berry and N. L. Balazs, Nonspreading wave packets, Am. J. Phys. **47**, 264 (1979).

[33] G. A. Siviloglou, J. Broky, A. Dogariu, and D. N. Christodoulides, Observation of accelerating airy beams, Phys. Rev. Lett. **99**, 213901 (2007).

[34] J. Broky, G. A. Siviloglou, A. Dogariu, and D. N. Christodoulides, Self-healing properties of optical Airy beams, Opt. Lett. **16**, 12880 (2008).

[35] G. A. Siviloglou, J. Broky, A. Dogariu, and D. N. Christodoulides, Ballistic dynamics of Airy beams, Opt. Lett. **33**, 207 (2008).

[36] M. Henstridge, C. Pfeiffer, D. Wang, A. Boltasseva, V. M. Shalaev, A. Grbic, and R. Merlin, Synchrotron radiation from an accelerating light pulse, Science **362**, 439 (2018).

[37] P. Polynkin, M. Kolesik, J. V. Moloney, G. A. Siviloglou, and D. N. Christodoulides, Curved plasma channel generation using ultraintense airy beams, Science **324**, 229 (2009).

[38] J. Shu, J. C. Vaughan, and X.-W. Zhuang, Isotropic three-dimensional super-resolution imaging with a self-bending point spread function, Nat. Photon. **8**, 302 (2014).

[39] J. Baumgartl, M. Mazilu, and K. Dholakia, Optically mediated particle clearing using Airy wavepackets, Nat. Photon. **2**, 675 (2008).

[40] A. Pukhov, Three-dimensional electromagnetic relativistic particle-in-cell code VLPL (Virtual Laser Plasma Lab), J. Plasma Phys. **61**, 425 (1999).

[41] D. M. Greenberger, Comment on "Nonspreading wave packets", Am. J. Phys. **48**, 256 (1980).

[42] H.-H. Liu, W.-M. Hao, X. Yin, S.-Q Chen, and L. Chen, Broadband generation of airy beams with hyperbolic metamaterials, Adv. Opt. Mater. **7**, 1900493 (2019).

[43] T. Ellenbogen, N. Voloch-Bloch, A. Ganany-Padowicz, and A. Arie, Nonlinear generation and manipulation of Airy beams, Nat. Photon. **3**, 395 (2009).

[44] N. Zaïm, D. Guénot, L. Chopineau, A. Denoeud, O. Lundh, H. Vincenti, F. Quéré, and J. Faure, Interaction of ultraintense radially-polarized laser pulses with plasma mirrors, Phys. Rev. X **10**, 041064 (2020).

[45] D. Abdollahpour, S. Suntsov, D. G. Papazoglou, and S. Tzortzakis, Spatiotemporal Airy light bullets in the linear and nonlinear regimes, Phys. Rev. Lett. **105**, 253901 (2010).

[46] B. Dromey, D. Adams, R. Hörlein, Y. Nomura, S. G. Rykovanov, D. C. Carroll, P. S. Foster, S. Kar, K. Markey, P. McKenna, D. Neely, M. Geissler, G. D. Tsakiris, and M. Zepf, Diffraction-limited performance and focusing of high harmonics from relativistic plasmas, Nat. Phys. **5**, 146 (2009).

[47] H. Vincenti, S. Monchocé, S. Kahaly, G. Bonnaud, Ph. Martin, and F. Quéré, Optical properties of relativistic plasma mirrors, Nat. Commun. **5**, 3403 (2014).

[48] H. Kallala, F. Quéré, and H. Vincenti, Techniques to generate intense isolated attosecond pulses from relativistic plasma mirrors, Phys. Rev. Res. **2**, 043007 (2020).

[49] J. Gao, B. Li, F. Liu, Z.-Y. Chen, M. Chen, X. Ge, X. Yuan, L. Chen, Z. Sheng, and J. Zhang, Divergence control of relativistic harmonics by an optically shaped plasma surface, Phys. Rev. E **101**, 033202 (2020).